DOI: 10.1002/ejic.201100335

$Mg_{11}Cu_6Al_{12}$, A New Link in the Structural Chemistry of $MgCu_2$-Type Clusters

Veronica M. Berns,[a] Timothy E. Stacey,[a] Michael Sapiro,[a] and Daniel C. Fredrickson*[a]

Dedicated to Professor John D. Corbett on the occasion of his 85th birthday

Keywords: Solid-state structures / Structure elucidation / Intermetallic phases / Magnesium / Copper / Aluminium

We report the synthesis and crystal structure of a new phase in the Mg-Cu-Al system: $Mg_{11}Cu_6Al_{12}$. This compound crystallizes in the $K_{17}In_{41}$ structure type. When written as $Mg_{17-x}Cu_xAl_{12}$, $x = 6$, the composition of this phase foretells a connection to $Mg_{17}Al_{12}$ (α-Mn type). The structures of both can be constructed from 29-atom fragments of the $MgCu_2$ structure type. They differ in the orientations of these fragments: the $Mg_{11}Cu_6Al_{12}$ structure is obtained when half of the $MgCu_2$-type clusters of $Mg_{17}Al_{12}$ are rotated by 90°. Electronic structure calculations using density functional theory (DFT) and the extended Hückel (eH) method point to driving forces for this structural transformation. Density of states (DOS) curves calculated for $Mg_{11}Cu_6Al_{12}$ in the two structure types indicate that both are stabilized by DOS minima close to the Fermi energy, with the pseudogap being deeper for the observed structure. An eH relative Mulliken population analysis reveals that cluster rotation also changes the electronic character of the outermost sites of the $MgCu_2$-type fragments: six atoms per formula unit go from being ambiguous to anionic, and thus suitable to occupation by relatively electronegative elements. These are the positions occupied by Cu in $Mg_{11}Cu_6Al_{12}$. The creation of these six anionic sites adapted to occupation by Cu provides an impetus for cluster rotation. The removal of ambiguity of the outermost sites of the $MgCu_2$-type fragments creates extended networks of anionic and cationic sites in $Mg_{11}Cu_6Al_{12}$. The cationic sites trace out the clathrate II framework noted by Corbett and coworkers in the $K_{17}In_{41}$ type, while the anionic sites ensheathe this framework to complete Friauf polyhedra around the framework atoms.

I. Introduction

Perhaps the first indication of the diversity that Nature offers in the field of intermetallic phases is found in Linus Pauling's X-ray diffraction investigations of $NaCd_2$ in 1923.[1] It would be almost 40 years of developing experience with intermetallics before Linus Pauling's associate Sten Samson would solve the structure of this phase, revealing a giant F-centered cubic unit cell of 30.56 Å containing more than one thousand atoms.[2,3] Since then, the theme of giant cubic unit cells has continued to expand. $NaCd_2$ has been joined by not only the closely related structures of β-Mg_2Al_3[4] and Cd_3Cu_4,[5] but also by the exponentially more complex structures of $Al_{56.5}Cu_{3.9}Ta_{39.5}$ (*cF*5908) and $Al_{55.4}Cu_{5.4}Ta_{39.1}$ (*cF*23134).[6,7] Our ability to solve the complex crystal structures of these phases has greatly improved since Pauling's original experiments on $NaCd_2$, but the chemical bonding factors underlying the formation of these incredible structures remain mysterious.

In this paper, we describe an attempt to probe their origins experimentally. This attempt is based on the observation of a shared feature of these phases: they all contain large blocks of the cubic Laves phase structure type, the $MgCu_2$ type.[8–10,6,7] We wondered how tunable these blocks might be, and whether it is possible to enlarge or shrink them through, say, elemental substitution. A simple way to approach this would be to examine ternary systems which contain both Laves phases and one of these complex cubic structures. For instance, the Mg-Cu-Al system contains both the classic Laves phase $MgCu_2$ and the monumental β-Mg_2Al_3 compound, as well as other phases based on Laves structure fragments, such as $Mg_{17}Al_{12}$ (ordered variant of the α-Mn type),[11,12] $Mg_{23}Al_{30}$,[13] and the low temperature rhombohedral form of Mg_2Al_3, the β′ phase.[14] Mg atoms and Cu/Al atoms play similar roles in all of these phases: the Mg atoms form the vertices of diamondoid (D) networks, while the Al/Cu atoms trace out networks including truncated tetrahedra (TT). Could partial replacement of Cu for Al in the Mg-Al phases enlarge their $MgCu_2$-type fragments?

After asking this question, we were excited to find that the Mg-Cu-Al phase diagram exhibits a phase with an unknown crystal structure, $Mg_6Cu_3Al_7$,[15–17] and we set out to synthesize it and solve its structure. As we will describe below, this endeavor resulted in crystals of the new phase

[a] Department of Chemistry, University of Wisconsin-Madison, 1101 University Avenue, Madison, WI 53706-1322, USA
E-mail: danny@chem.wisc.edu

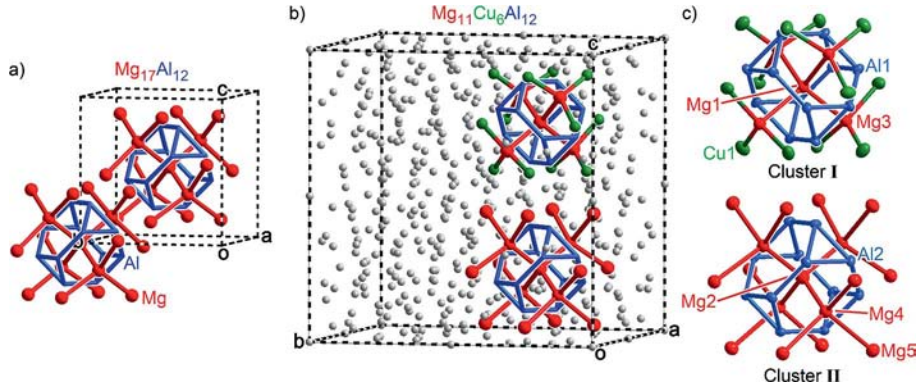

Figure 1. $MgCu_2$-type fragments in the $Mg_{17}Al_{12}$ (α-Mn type) and $Mg_{11}Cu_6Al_{12}$ structures. (a) The crystal structure of $Mg_{17}Al_{12}$, with the $MgCu_2$-type fragments at one unit cell corner and the cell center drawn. Red spheres indicate Mg atoms corresponding to Mg-occupied positions in the $MgCu_2$ type, and blue bars trace out connections between Al atoms, which correspond to Cu-occupied positions in the $MgCu_2$ type. (b) The two symmetry distinct $MgCu_2$-type fragments in $Mg_{11}Cu_6Al_{12}$, presented in the context of the full unit cell. Both are closely analogous to the fragments in (a). (c) The $MgCu_2$-type fragments of $Mg_{11}Cu_6Al_{12}$ drawn individually, with site labels, and thermal ellipsoids plotted at the 99% probability level. Each symmetry-inequivalent site belongs to one of these two fragments.

$Mg_{11}Cu_6Al_{12}$, a ternary variant of the $K_{17}In_{41}$ structure type[18–20] as shown in Figure 1. In our examination of its crystal structure, we realized that we had, in the words of Prof. John Corbett, done the right experiment for the wrong reasons. We will see that, rather than leading to a path between the Laves phases and Samson's giant cubic phase β-Mg_2Al_3, $Mg_{11}Cu_6Al_{12}$ reveals an intimate link between two structures based on $MgCu_2$-type fragments: the $K_{17}In_{41}$ and the α-Mn structure types. In doing so, this phase will show us one mechanism by which complex intermetallic superstructures can have simple origins.

II. Synthetic Results: Identification of $Mg_{11}Cu_6Al_{12}$

As we described above, our original synthetic target was the $Mg_6Cu_3Al_7$ phase indicated by the Al-Mg-Cu phase diagram,[15–17] whose 12.09 Å body-centered cubic unit cell was originally assigned from X-ray diffraction data by Mirgalovskaya in 1951,[21] and was more recently observed in electron diffraction data.[22,23] The results of our synthetic work (described in detail in the Technical Procedures section at the end of this paper) could be readily understood from the position of the $Mg_6Cu_3Al_7$ composition being under the primary phase-field of Laves phase structures. Syntheses involving slow cooling from a molten mixture of the elements resulted in multi-phase samples, from which crystals for single-crystal X-ray diffraction work could be obtained. Quenching from the melt followed by annealing below the liquidus provided samples with much greater phase purity, with the principle impurity being a $MgZn_2$-type phase which presumably crystallized out as the sample passed through the liquidus during the quench. The only crystals observed under these synthetic conditions were of the $MgZn_2$-type phase.

The powder X-ray diffraction patterns exhibited peaks which matched some of the low angle peaks reported for the $Mg_6Cu_3Al_7$ phase in the ICDD Powder Diffraction File. However, in our single-crystal X-ray diffraction analysis of numerous crystals we never obtained this cell. Instead, we repeatedly encountered a 20.1 Å cubic unit cell, as well as a 5.6 Å × 5.6 Å × 8.4 Å hexagonal unit cell. After collecting full data sets and carrying out structure solutions and refinements (see experimental procedures) on crystals of these phases, the cubic cell was revealed to belong to a phase whose atomic positions matched the $K_{17}In_{41}$ type. The hexagonal cell was found to belong to a $MgZn_2$-type structure. WDS measurements gave approximant compositions for these phases as respectively $Mg_{11.30(11)}Cu_{6.00(9)}Al_{12.86(11)}$ and $Mg_{32(2)}Cu_{38(4)}Al_{30(6)}$. Virtually all peaks in the experimental powder patterns for our highest purity samples could be assigned to one of these phases.

One interpretation of these results can be found by comparing our synthetic conditions with the original conditions used by Mirgalovskaya in the preparation of $Mg_6Cu_3Al_7$.[21] Mirgalovskaya's synthesis involved annealing at 400 °C for 45 days, whereas the minimum annealing temperature in our syntheses so far has been 450 °C. It seems possible that Mirgalovskaya's $Mg_6Cu_3Al_7$ compound is a lower temperature phase occurring below the liquidus.

III. The Crystal Structure of $Mg_{11}Cu_6Al_{12}$ by Comparison with $Mg_{17}Al_{12}$

While our initial goal was to investigate $Mg_6Cu_3Al_7$, our focus shifted to the new $Mg_{11}Cu_6Al_{12}$ phase we encountered. This phase crystallizes in the $K_{17}In_{41}$ type, a structure type that has been described in a variety of ways: in terms of Bergman clusters,[24] as a framework of deltahedral clusters connected via exo-bonds,[25] as being built from $MgCu_2$-type fragments,[10] and in terms of a clathrate II framework.[20,25] Our original interest in the Mg-Cu-Al ternary system was due to its potential to bridge the Laves phase fragments in the Al-Mg system and the classic $MgCu_2$ Laves phase in the Mg-Cu system. This leads us to seek structural connections between $Mg_{11}Cu_6Al_{12}$ and

these known compounds. Looking through the list of Al-Mg phases reveals a compound with a close compositional relationship to the new $Mg_{11}Cu_6Al_{12}$ phase: $Mg_{17}Al_{12}$. The $Mg_{11}Cu_6Al_{12}$ stoichiometry can be obtained from $Mg_{17}Al_{12}$ by simply replacing six Mg atoms with Cu.

This similarity in stoichiometry stems from a deeper structural relationship between these two phases. Let's start by reviewing the structure of $Mg_{17}Al_{12}$. This phase forms an ordered binary variant of the α-Mn structure. A simple, quantum mechanically derived way of viewing this structure has previously been presented.[10] In this view, the structure is constructed from fragments of the simple $MgCu_2$ type (Figure 1, a). These fragments can be decomposed into two networks: truncated tetrahedra (TT) corresponding to Cu-occupied sites in the $MgCu_2$-type (blue), and diamondoid (D) networks (red) interpenetrating the TT network corresponding to Mg-occupied sites in the $MgCu_2$ type. Each fragment contains 12 Al atoms on the TT sites, and 17 Mg atoms on the Mg sites to give the phase's $Mg_{17}Al_{12}$ stoichiometry. This model accounts for all atoms in the unit cell uniquely.

Analogous 29-atom $MgCu_2$-type fragments can be identified in the $Mg_{11}Cu_6Al_{12}$ phase. Two symmetry inequivalent fragments occur, labeled as clusters **I** and **II**. These are shown in the context of the full unit cell in Figure 1 (b), and separately with thermal ellipsoids in Figure 1 (c). Just as in $Mg_{17}Al_{12}$, all symmetry inequivalent sites of the structure can be mapped to these 29-atom $MgCu_2$-type fragments.

It then becomes natural to discuss $Mg_{11}Cu_6Al_{12}$ in terms of its differences from the structure of $Mg_{17}Al_{12}$. These can be expected to be of two kinds: (1) differences in the details of the $MgCu_2$ fragments, and (2) differences in their packing to form the full unit cell of the structure. Differences of the first kind are readily apparent in Figure 1. Whereas cluster **II** shows a close correspondence to the $Mg_{17}Al_{12}$ cluster, with all TT sites being occupied by Al and all the D sites with Mg, cluster **I** shows a somewhat different site-coloring. All TT sites are still occupied by Al, and in the innermost D sites are still filled by Mg, but now the outermost D sites are occupied by Cu. This distribution of both Mg and Cu over the D sites and the exclusive occupation of TT sites by Al leads to the $(Mg/Cu)_{17}Al_{12}$ stoichiometry noted above.

The differences in the packing of these clusters are shown in Figure 2. These differences can be simply derived with the following construction: We begin with a $2\times2\times2$ supercell of $Mg_{17}Al_{12}$, as shown in Figure 2 (a). Here we have taken a simplified view in which the $MgCu_2$ fragments are abbreviated as truncated tetrahedra. We then resolve the body-centered packing of fragments into two interpenetrating diamond networks, one drawn in blue, the other in

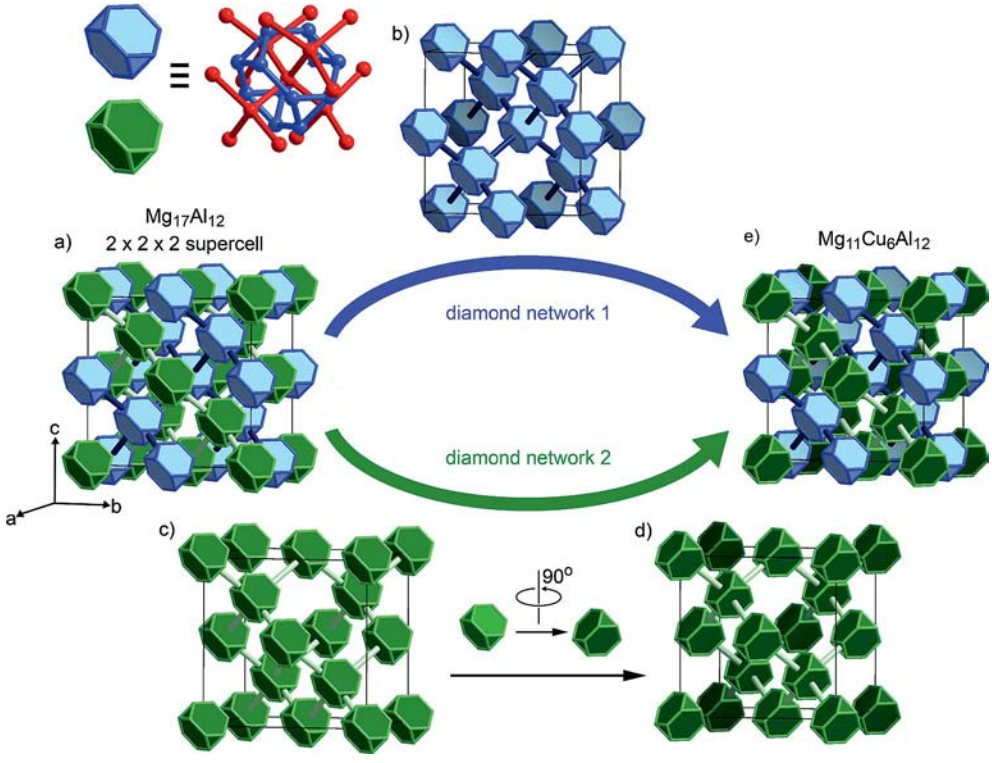

Figure 2. The structural transformation connecting $Mg_{17}Al_{12}$ (α-Mn type) to $Mg_{11}Cu_6Al_{12}$. (a) A $2\times2\times2$ supercell of $Mg_{17}Al_{12}$, with two diamond networks of $MgCu_2$-type clusters (abbreviated here as truncated tetrahedra) differentiated with blue (diamond network 1) and green (diamond network 2). (b) Diamond network 1 remains unchanged during the transformation. (c) The $MgCu_2$-type clusters of the diamond network 2 are rotated 90° about the *c*-axis to produce (d) a new diamond network with its $MgCu_2$-type clusters in a new orientation. (e) Recombining the unchanged network 1 with the transformed network 2 results in the $MgCu_2$-type cluster packing of the $Mg_{11}Cu_6Al_{12}$ structure.

green. These two networks are drawn separately in Figure 2 (b and c). Next, we rotate each of the clusters in the network in green 90° about the *c*-axis, creating a new diamond network with the fragments in a new orientation (Figure 2, d). Finally, we remerge the two diamond networks – one unchanged, one with rotated fragments – into a double diamond framework to arrive at the fragment packing of $Mg_{11}Cu_6Al_{12}$ (Figure 2, e).

This transformation has consequences for the symmetry of the structure. In $Mg_{17}Al_{12}$, the networks drawn in blue and green are made equivalent by the lattice translations of the crystal. Cluster rotation to produce $Mg_{11}Cu_6Al_{12}$ breaks this translational symmetry, generating a $2\times2\times2$ supercell. The blue and green networks are no longer translationally equivalent. Instead, they are now related through the *d*-glides of the $Fd\bar{3}m$ space group.

What is accomplished in terms of increased stability through the transformation? In the next sections, we will begin to see clues to the answer of this question, as we investigate the electronic structure of $Mg_{11}Cu_6Al_{12}$ through theoretical calculations using both Density Functional Theory (DFT) and the semi-empirical extended Hückel method.

IV. Pseudogap Stabilization of $Mg_{11}Cu_6Al_{12}$

In the above structure analysis, we uncovered a simple relationship between the crystal structure of the newly determined $K_{17}In_{41}$-type phase $Mg_{11}Cu_6Al_{12}$ and that of $Mg_{17}Al_{12}$. The atomic positions for the former may be obtained from the latter by a rotation of half of its $MgCu_2$-type clusters by 90° about the *c*-axis. By comparing the stoichiometries of the two compounds, it appears that this rotation is driven by the substitution of 6 Mg atoms/formula unit with Cu. How does such a substitution drive this structural change? Previous work on the $K_{17}In_{41}$ structure type suggests that electron count may be playing a role here. In their analysis of the isostructural phase $Mg_{35}Cu_{24}Ga_{53}$, Lin and Corbett found that this structure can be viewed as a network of deltahedral clusters interconnected by exobonds, with spectator atoms occupying the interstitial spaces of this network.[25] This suggested that the Zintl approach, employing the Wade-Mingos rules to the expected electron counts of the deltahedral clusters, should be applicable. The valence electron count was indeed very close to that predicted from the Zintl model, with the mismatch in electron counts being only 0.22 or 0.54%, depending on the sample.

As Mg is substituted with Cu to go from $Mg_{17}Al_{12}$ to $Mg_{11}Cu_6Al_{12}$, each atom replaced lowers the valence electron count by one (viewing Mg and Cu as respectively $3s^2$ and $4s^1$ metals). One hypothesis for the origin of the structural transformation is that this lowering of the electron count tunes the E_F to match a pseudogap for the electronic density of states (DOS) curve for the $K_{17}In_{41}$-type structure. To explore this possibility, we performed GGA-DFT calculations on a series of structures connecting $Mg_{17}Al_{12}$ to $Mg_{11}Cu_6Al_{12}$: (1) $Mg_{17}Al_{12}$, (2) a phase with the composition $Mg_{11}Cu_6Al_{12}$ but the α-Mn-type structure of $Mg_{17}Al_{12}$, with Cu atoms placed on the outermost D sites of one of the two $MgCu_2$-type fragments in the body-centered unit cell, and (3) the $Mg_{11}Cu_6Al_{12}$ structure. Calculation of DOS curves was performed for each phase on structures energy-minimized with GGA-DFT (the details of the calculations are provided in the Experimental Section).

The DOS curves from the DFT-optimized structures are presented in Figure 3. Perhaps the most notable differences occurring among these curves is the presence of a sharp DOS peak at ca. –9 eV for those structures containing Cu, and its absence in those structures without Cu. This peak corresponds to the Cu 3*d* orbitals, whose narrow distribution along the energy axis suggests that they may be considered as largely core-like.

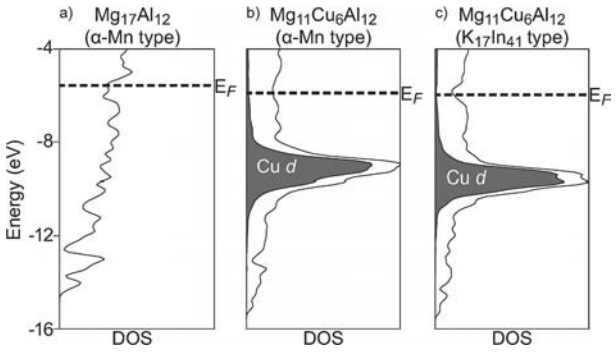

Figure 3. Density of states (DOS) curves calculated at the GGA-DFT level for (a) $Mg_{17}Al_{12}$ in its α-Mn-type structure, (b) $Mg_{11}Cu_6Al_{12}$ in the α-Mn type, and (c) $Mg_{11}Cu_6Al_{12}$ in the experimentally observed $K_{17}In_{41}$ type. The Fermi energy (E_F) for each is represented with a dashed line. Note that in all three DOS curves, the E_F lies in a depression of the DOS. This pseudogap is optimized for $Mg_{11}Cu_6Al_{12}$ in the $K_{17}In_{41}$ type (c). In (b) and (c), the shaded areas give the projected density of states for the Cu *d* states. In order to bring out the overarching features of the DOS distributions, the presented curves have been treated with Gaussian broadening.

When the presence or absence of the Cu 3*d* peak is disregarded, the DOS curves display some similarity. Each of them shows a largely parabolic distribution, characteristic of nearly-free-electron *sp* states. Each curve also shows an DOS depression near the E_F at about –5.5 eV, suggestive of a special stability at these electron counts. The deeper pseudogap afforded by $Mg_{11}Cu_6Al_{12}$ in the $K_{17}In_{41}$ type would be expected to provide a driving force for the structural transition.

V. Relative Mulliken Population Analysis of the $MgCu_2$-Type Clusters in $Mg_{11}Cu_6Al_{12}$

A much simpler quantum mechanical approach – the relative Mulliken population analysis – can lead us to a more dramatic driving force for the structural transition. In this approach, one uses quantum mechanical calculations (usually of the extended Hückel type) on an elemental model of a phase to probe the impetus for elemental substitution in

its structure. This technique was pioneered in the field of organic chemistry,[26,27] where it was noted that carbon atoms appearing as (slightly) anionic in calculations on hydrocarbons were found to be most easily substituted by more electronegative heteroatoms, while those showing cationic charges were most easily replaced by more electropositive elements. This observation was termed Topological Charge Stabilization (TCS). Later, this approach was applied to intermetallic phases, providing insights into and predictions of site-preferences,[28,29] and guidance for those navigating the multitude of possible descriptions of complex crystal structures.[10,30,31]

Let's start with a review of what this type of analysis tells us about the $Mg_{17}Al_{12}$ structure,[10] for contrast with the results we will find for $Mg_{11}Cu_6Al_{12}$. For this analysis, we first perform an extended Hückel (eH) calculation on an elemental model of $Mg_{17}Al_{12}$, with the valence electron concentration adjusted to match that of $Mg_{17}Al_{12}$, i.e. $(2\times17 + 3\times12)/(17 + 12) = 2.41$ electrons/atom. This is envisioned as representing a version of this phase without Al/Mg ordering, but in practice is achieved by beginning with Al eH parameters and tuning them to achieve a qualitative match with a band structure calculated with DFT. After the eH calculation is carried out, Mulliken populations are extracted, and charges are calculated relative to the average electron count, yielding relative Mulliken populations.

The result for $Mg_{17}Al_{12}$ is plotted in Figure 4 (a), where following earlier conventions, the relative Mulliken populations are represented with spheres. White spheres indicate sites that are more anionic than the average electron count, while black spheres indicate those that are more cationic that the average. The volumes of the spheres are proportional to the magnitudes of the charges. In this plot, the differences in electronic character between the atoms of the TT sites and the D sites are readily apparent. The TT sites are exclusively decorated by white spheres, indicating that these are relatively anionic. The D sites, on the other hand, are decorated with black spheres; these are relatively cationic.

From this plot, several things can be learned about the electronic structure of this phase. First are the affinities of the sites for relatively electronegative vs. electropositive atoms. Following the logic of TCS, the most electronegative atoms are expected to go to the most electron-rich sites in an elemental calculation. This is indeed the case: of Al and Mg, Al is the more electronegative, and this element is observed to occupy the relatively anionic sites, while Mg is relegated to the remaining relatively cationic sites.

We also gain insights into structural connections between intermetallic structure types. A cationic D network interpenetrating an anionic TT network is also seen in the much simpler and more common $MgCu_2$ structure, where the D network extends throughout the structure as a full diamond lattice, and the TT network forms an infinite network of vertex-sharing tetrahedra. These networks appear in truncated form not only in $Mg_{17}Al_{12}$, but also in Mulliken population analyses of the more complex $NaCd_2$, and β-Mg_2Al_3 structures. Relative Mulliken population analysis places these phases into a structural series based on Laves phase fragments.

Finally, relative Mulliken population analysis provides us with a sense of the texture of the crystal structure. Near the centers of the $MgCu_2$-type fragments, the spheres representing relative charges are comparatively large, indicating that these sites show a strong preference for either Al or Mg. Toward the boundaries of the fragment, however, this preference becomes much weaker: the outermost atoms now exhibit tiny black spheres. This weaker preference can be traced to the geometry at the interfaces between clusters. While these sites are drawn connected to the D networks of their $MgCu_2$-type fragments, they can also be viewed as continuing the TT networks of the neighboring clusters (Figure 5, a). This ambiguity leads to a difference in bond-

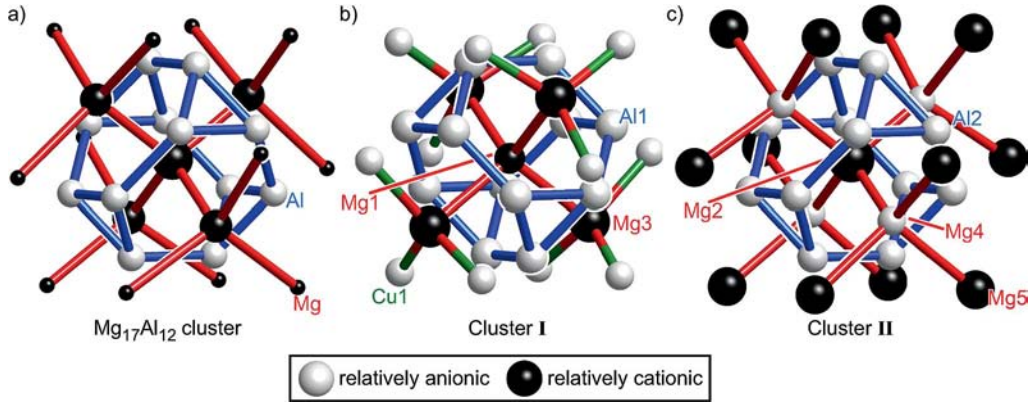

Figure 4. Relative Mulliken population distributions over the $MgCu_2$-type fragments occurring in (a) $Mg_{17}Al_{12}$ and $Mg_{11}Cu_6Al_{12}$ at the (b) cluster **I** and (c) cluster **II** positions. Mulliken populations were extracted from extended Hückel calculations on elemental models of the $Mg_{17}Al_{12}$ and $Mg_{11}Cu_6Al_{12}$ structures (see text for details). Sites that are anionic relative to the average electron count are indicated with white spheres, while relatively cationic sites are shown with black spheres. The magnitude of the relative charge is proportional to the volumes of the spheres. In general, the TT networks are drawn in blue, while D networks are shown in red. Due to the importance that Cu occupation will take in the story to come, Cu positions are indicated with green regardless of their assignment to TT or D networks. These conventions will be used throughout this paper.

ing character between the more central atoms of the cluster, where sites are relatively polar (relative Mulliken populations larger in magnitude, whether positive or negative), and the outer atoms of the cluster, where sites are relatively nonpolar (relative Mulliken populations smaller in magnitude).

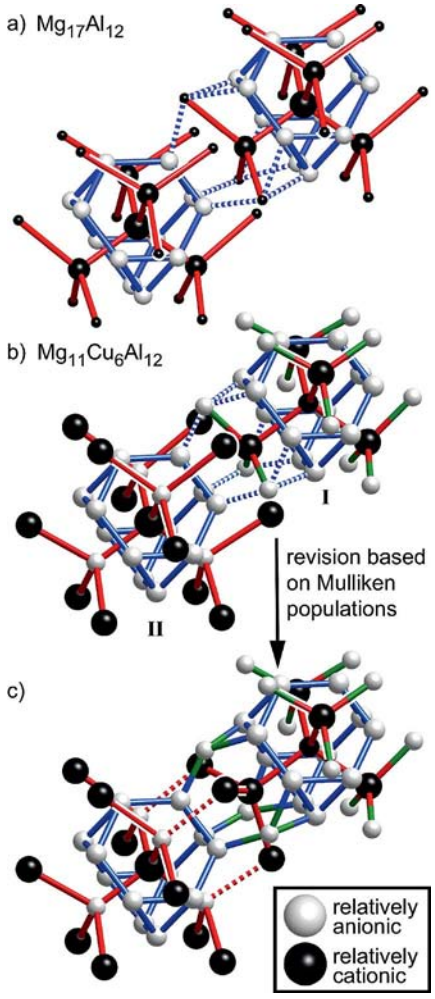

Figure 5. The triangle-facing-hexagon (TfH) interfaces between $MgCu_2$-type fragments in $Mg_{17}Al_{12}$ and $Mg_{11}Cu_6Al_{12}$. (a) Mulliken population analysis of TfH interfacial regions in $Mg_{17}Al_{12}$. (b) Mulliken population analysis of the $MgCu_2$-type clusters meeting at a TfH interface in $Mg_{11}Cu_6Al_{12}$, and (c) revised site network assignments based on the signs of the relative Mulliken populations. See caption to Figure 4 for plotting conventions.

To what extent do these conclusions also apply to $Mg_{11}Cu_6Al_{12}$? In Figure 4 (b and c), we overlay spheres corresponding to relative Mulliken populations on the sites of clusters **I** and **II** of this phase, respectively. For both clusters, similarities and differences are seen when compared to the fragments in $Mg_{17}Al_{12}$ and to each other. In all three clusters, the central D atom appears as cationic, and the surrounding TT sites are relatively anionic. The main differences are seen in the charges of the sites further from the fragment centers. While the D sites immediately adjacent to the central site are cationic as expected in cluster **I**, the corresponding sites in cluster **II** now appear as anionic. The outermost sites show differences that are just as significant: the small black spheres at the fringes of the fragment in $Mg_{17}Al_{12}$ have given rise in $Mg_{11}Cu_6Al_{12}$ to large black spheres for cluster **II** and large white spheres for cluster **I**. The nonpolar cluster exterior sites of $Mg_{17}Al_{12}$ have split into two types of polar sites in $Mg_{11}Cu_6Al_{12}$ with opposite charges. During the transformation between these two structure types presented in Figure 2, the ambiguities in the assignments of these sites seem to have been resolved.

VI. New Connectivities at the Interfaces between $MgCu_2$-Type Clusters

Evidently, quantum mechanics is directing us to reevaluate our descriptions of the atoms at the fragment exteriors in $Mg_{11}Cu_6Al_{12}$. To do this, we now change our focus from individual clusters to the interfaces between them. In $Mg_{17}Al_{12}$, only one type of interface occurs: each triangular face of the TT of one cluster lies opposite to a hexagonal face of the TT network of a neighboring cluster (Figure 5, a). In $Mg_{11}Cu_6Al_{12}$, by contrast, several different types of interfaces are present. As we saw in Figure 2, the packing of $MgCu_2$ clusters in this phase can be represented by two interpenetrating diamond networks, related by *d*-glide symmetry. Within each of these networks the interfaces remain closely analogous to those in $Mg_{17}Al_{12}$: TT triangles face TT hexagons with Friauf polyhedra occurring at the interface. Between the clusters of different networks, on the other hand, new interfaces arise. At half of these interfaces, TT triangles face TT triangles; at the other half TT hexagons meet TT hexagons. We will designate these interface types as respectively triangle-facing-hexagon (TfH), triangle-facing-triangle (TfT), and hexagon-facing-hexagon (HfH).

Let's begin with the interface type shared with the $Mg_{17}Al_{12}$ structure, the TfH interface. In Figure 5, we show two clusters meeting at one of these interfaces for both the $Mg_{17}Al_{12}$ (Figure 5, a) and the $Mg_{11}Cu_6Al_{12}$ (Figure 5, b) structures. In both structures, the outermost D sites of the clusters coming from the left and right play different roles at this interface. Those from the right cluster form contacts that bridge the TT networks of the two clusters, as is shown with dashed blue lines. These complete a new TT at the interface. The outermost D sites of the left cluster belong to a D network that threads through the interfacial TT network. Together these features form a Friauf polyhedron at the cluster interface in both structures.

Despite these geometrical similarities, the relative Mulliken populations at the TfH interfaces show significant differences between $Mg_{17}Al_{12}$ and $Mg_{11}Cu_6Al_{12}$. In $Mg_{17}Al_{12}$ (Figure 5, a), the symmetry equivalence of the outermost D sites means that they are not well-adapted to their roles in either the D network or the TT network. This is seen in their relative Mulliken populations, which appear here as tiny black spheres, with their small size indicating small magnitudes of relative charge. In $Mg_{11}Cu_6Al_{12}$ (Figure 5, b), the clusters coming from the right and left are symmetry

inequivalent. The one coming from the left is an instance of cluster **II**, while that from the right is an instance of cluster **I**. As these clusters are not related by symmetry, neither are their outermost D sites. This has a profound effect on the Mulliken populations. The sites contributing to the interfacial TT network from cluster **I** now show strong anionic character, while those contributing to the D network of the interfacial Friauf polyhedron show clear cationic character. Both changes are consistent with the assignment of these sites to the networks of the interfacial Friauf polyhedron.

From this analysis, we are led to revise our assignments of these interfacial sites in $Mg_{11}Cu_6Al_{12}$, as shown in Figure 5 (c). In this new view of the structure, the outermost D sites of cluster **II** remain assigned as D sites, but are now viewed as unambiguously belonging to the D network connecting clusters **I** and **II**. The corresponding sites of Cluster **I** are now viewed as TT sites bridging the TT networks of the two clusters.

VII. Another Driving Force for Adopting the Structure of $Mg_{11}Cu_6Al_{12}$

This is far from the last word that the Mulliken populations will have to tell us about the optimal description of this structure, but at this point we can already understand why this structure might be preferred over that of $Mg_{17}Al_{12}$ for the composition $Mg_{11}Cu_6Al_{12}$. Consider the creation of this phase beginning with $Mg_{17}Al_{12}$ and then substituting some of its Mg sites with Cu to attain the $Mg_{11}Cu_6Al_{12}$ stoichiometry. Cu is of greater electronegativity than both Al and Mg. If Cu is constrained to substitute for Mg as per the stoichiometry, it would be expected to substitute for the most electron-rich of the Mg-sites. These are the outermost D sites of the $MgCu_2$-type clusters. If the $Mg_{17}Al_{12}$ structure were to be retained, however, the structure would offer no differentiation between those sites to be occupied by Cu and those to remain Mg. Upon moving to the $Mg_{11}Cu_6Al_{12}$ structure type, this issue is solved with the resolution of the outermost D positions into two sets, one set more appropriate for relatively electronegative elements, the other set better suited to more electropositive elements.

This is indeed seen in the site occupancies. In $Mg_{11}Cu_6Al_{12}$, those outermost D sites that are now firmly established as electropositive D network atoms continue to be occupied by Mg. The sites that we have reassigned to interfacial TT networks, based on their clear anionic character in the Mulliken populations, are occupied by Cu atoms. The stability thus seems to be related to the removal of the ambiguity in the site identities of the outermost D atoms on going from the $Mg_{17}Al_{12}$ structure to that of $Mg_{11}Cu_6Al_{12}$.

VIII. More Interfaces, More New Connectivities

What are the changes in the environments of these sites that have removed their ambiguous identities? To answer this question, we now turn to the remaining interface types in this structure: the TfT and HfH interfaces. These interfaces are shown, along with their Mulliken populations, in Figures 6 and 7, respectively. From looking at the identities of the clusters involved in the interfaces, an important dif-

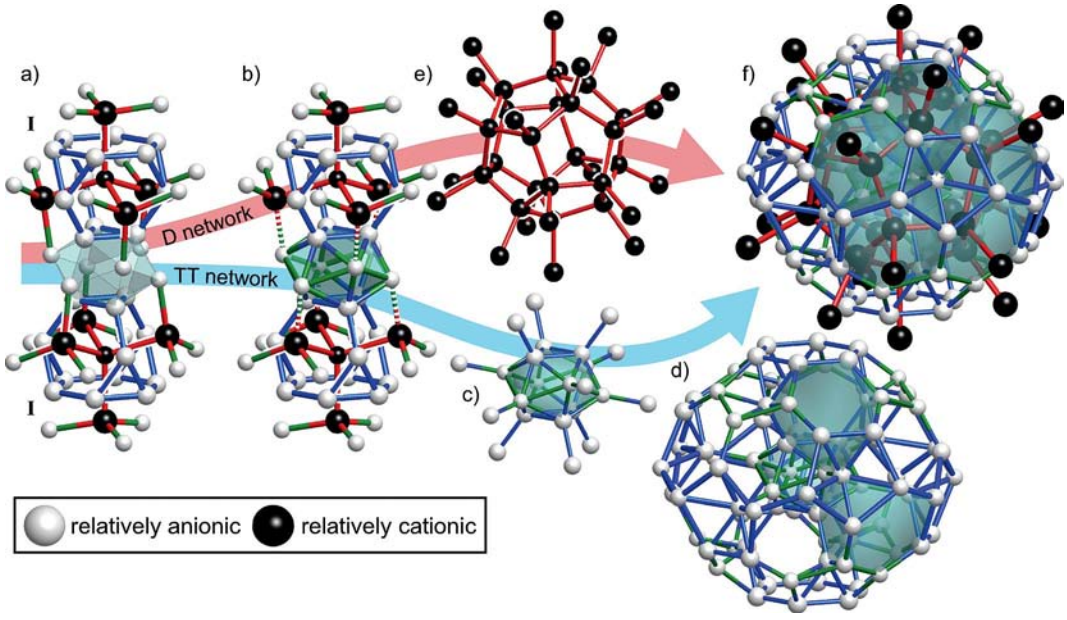

Figure 6. Triangle-facing-triangle (TfT) interfaces between $MgCu_2$-type fragments in $Mg_{11}Cu_6Al_{12}$. (a) TfT interfaces occur between two instances of cluster **I**. (b) Drawing connections between relatively anionic sites at the interface yields an empty icosahedron. (c)–(d) Following connections from this icosahedron to other anionic sites reveals a TT network consisting of a central icosahedron sharing all of its faces with truncated tetrahedra. The outer shell of this network is the familiar fullerene cage. (e) Tracing out the contacts between cationic sites surrounding the icosahedron in (b) creates a D network based on dodecahedra. (f) Combining the D and TT networks from (c)–(e) yields a Bergman cluster. Plotting conventions are given in the caption to Figure 4.

ference from the TfH interfaces becomes apparent. Whereas the clusters on opposites sides of the TfH interfaces were symmetry inequivalent – one being of the cluster **I** type, the other of the cluster **II** type – the clusters meeting at the TfT and HfH are now related by symmetry. At the TfT interfaces two type **I** clusters meet, while at the HfH interfaces two type **II** clusters face each other.

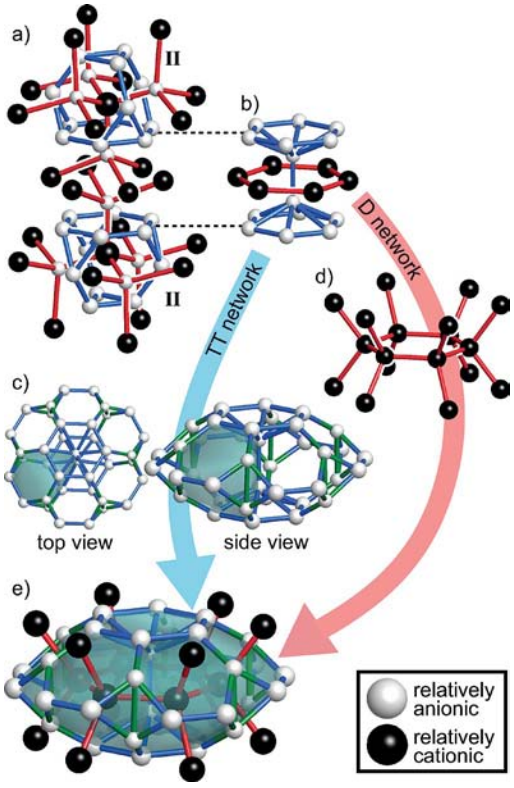

Figure 7. Hexagon-facing-hexagon (HfH) interfaces between $MgCu_2$-type fragments in $Mg_{11}Cu_6Al_{12}$. (a) Two instances of cluster **II** meeting at the HfH interface. (b) Assigning atoms at the interface to anionic and cationic networks reveals a grooved anionic hexagonal "car wheel," encircled by a cationic "tire." (c) Extending the TT contacts outward yields a hexagon of face-sharing truncated tetrahedra. (d) The D network that results from including further contains between cationic sites. (e) Merging the TT and D networks of (c) and (d), respectively, creates a hexagonal ring of Friauf polyhedra. Conventions used in the plots are described in the caption to Figure 4.

At the TfT interface, the Cu1 sites interdigitate and connect the triangular faces of their clusters to create an empty icosahedron (Figure 6, a–b). This icosahedron forms the center of the Bergman clusters that have been noted previously in this structure type.[24] In fact, tracing out connections between anionic sites starting from this interface polyhedron leads to an icosahedron of truncated tetrahedra, each sharing a triangular face with this central icosahedron (Figure 6, c–d). This is the TT network of a Bergman cluster. For the Cu1 sites, rather than have their TT character at the TfH interface deconstructively interfere with a D network at another interface as in the original $Mg_{17}Al_{12}$ structure, the TT character is reinforced by the larger structural context. In fact, their positions at the central icosahedron of a Bergman cluster means that each Cu1 site participates in not one but five truncated tetrahedra, one for each of the triangular faces of the icosahedron sharing that site.

The exclusive decoration of the Bergman cluster TT network by anionic sites in Figure 6 (c–d) indicates that this cluster is an electronically important feature of the $Mg_{11}Cu_6Al_{12}$ structure. This is confirmed by a look at the Bergman cluster's D network (Figure 6, e); all of the sites of this D network are relatively cationic. In Figure 6 (f), we show the full Bergman cluster with the relative Mulliken populations for each site. Again a clear segregation of the charges for the cluster is seen between a cationic D network and an anionic TT network.

From our analysis of the TfT interface, we have seen that the rotation of half of the $MgCu_2$-type clusters of the $Mg_{17}Al_{12}$ structure to create $Mg_{11}Cu_6Al_{12}$ has yielded a host of new Friauf polyhedra. The same theme is also observed at the HfH interface. The joining of the two $MgCu_2$-type clusters at the HfH interface is shown in Figure 7. Here, the D networks of the two clusters interdigitate in a similar way to the interface between symmetrically inequivalent $MgCu_2$ type clusters in $NaCd_2$.[10] In $NaCd_2$, this type of interface was noted to form a fragment of the Al_3Zr_4 structure type. This description applies geometrically here as well, but in following the Mulliken populations, a quite different view emerges.

We begin by noting that the Mg4 sites just above and below the TT hexagonal faces at the interfaces exhibit relative Mulliken populations uncharacteristic of D network sites. Sites assigned to D networks usually appear as cationic in these calculations, but here the Mg4 sites show clear anionic character, suggesting that they should be reassigned as TT sites. In doing so, we seek out connections to other nearby TT sites, as shown in Figure 7 (b). The Mg4 sites become connected to each other and to the hexagonal faces of the TT networks above and below, effectively becoming the axle between a pair of hexagonal wheels. Upon making this change, the remaining D atoms at the interface are left unconnected, unless we search for other possible D–D connectivities. The interdigitation of the two D networks stemming from the two $MgCu_2$-type clusters allows for such new connections (Figure 7, b); these trace out a hexagon around the pair of Mg4 sites.

From this close-up view, it is difficult to see how these patterns of relatively anionic and cationic sites should be interpreted. In Figure 7 (c–e), we zoom out to show the HfH interface sites in their larger structural context. Figure 7 (c) displays contacts between the anionic interfacial sites and other nearby anionic sites between the two $MgCu_2$-type clusters. The double hexagonal wheel of Figure 7 (b) manifests here as the intersection of six truncated tetrahedra arranged, via the sharing of hexagonal faces, into a sixfold ring. Seeking out contacts from the interfacial cationic sites also yields familiar features. In Figure 7 (d), we trace out connections from these sites to their nearest cationic neighbors in the immediate surroundings. The new contacts complete tetrahedral coordination of the interfa-

cial cationic sites by other cationic sites. This result is a hexagonal array of tetrahedra corresponding to a new D network.

When these anionic TT and cationic D networks are superimposed, the D network threads through the hexagonal faces of the TT network, creating Friauf polyhedra. The HfH interface thus serves at the meeting point of six Friauf polyhedra arranged in a ring. The Mulliken populations at this interface reflect their placement on either the TT (anionic) or D (cationic) networks of this ring of polyhedra.

From this conclusion, we can understand the somewhat puzzling appearance of Mg4 as an electron-rich site, despite its placement on the D network of one of the $MgCu_2$-type clusters originally identified in $Mg_{11}Cu_6Al_{12}$. The D network extending from the center of the $MgCu_2$-type cluster is just one network that the site takes part in. It also participates in the six truncated tetrahedra encircling the HfH interface. This TT network character dominates in the Mulliken population analysis. However, the partial D-character, while not apparent in the Mulliken population for the Mg4 site, may help explain why Mg occupies this site when the relative Mulliken population analysis predicts it to have an affinity for more electronegative atoms. Placement of Mg atoms at only the sites calculated as relatively cationic gives the stoichiometry $Mg_9(Cu/Al)_{20}$, quite Mg-deficient relative to the crystal structure's composition of $Mg_{11}(Cu/Al)_{18}$. The partial D-character of this site can be evoked to rationalize the placement of the excess Mg atoms on the Mg4 positions.

IX. A Quantum Mechanically-Derived View of $Mg_{11}Cu_6Al_{12}$, Featuring a Clathrate Framework

Now that we have examined all of the interface types occurring in $Mg_{11}Cu_6Al_{12}$, we would like to make an observation. Unlike $Mg_{17}Al_{12}$, where the blurred identities of the outermost D sites of the $MgCu_2$ clusters creates the impression of isolated clusters, no clear boundaries have been found so far to the TT and D networks identified by relative Mulliken populations in $Mg_{11}Cu_6Al_{12}$. In fact, these networks extend throughout the whole crystal, as shown in Figure 8. In part (a) of this graphic the D network formed from the cations is shown. This forms a space-filling arrangement of pentagonal dodecahedra and hexakaidecahedra, the two polyhedra that make up the clathrate II structure. Indeed, this network is the very clathrate II framework of cations that Corbett and co-workers identified previously in the $K_{17}In_{41}$ type.[20,25]

The relatively anionic sites ensheathe this cationic clathrate network, providing each cationic site with truncated tetrahedral coordination by anions. The D–D contacts of the clathrate network then pass through the hexagonal faces of the TT network. With this view in hand, many features already noted in this structure become easily interpretable (see part b of Figure 8). The Bergman clusters appearing at the TfT interfaces arise from the decoration of the dodecahedra of the clathrate framework with Friauf polyhedra. Similarly, the hexagonal rings of Friauf polyhedra identified at the HfH are created by the decoration of the hexagonal faces of the hexakaidecahedra.

Only one symmetry inequivalent site is yet to be accounted for in this clathrate framework description: the Mg2 site that forms the center of cluster **II**. In the D network of Figure 8 (b), these sites are represented by the isolated black spheres at the centers of the hexakaidecahedra. Recall that all of the Mg2 site's neighbors are anionic (Figure 4, c). As such, it exhibits no connectivity with the other D network atoms.

As this site centers a $MgCu_2$-type cluster, its coordination environment is a Friauf polyhedron. All of the other Friauf polyhedra in this structure can be described as decorating the clathrate framework. The presence of this one

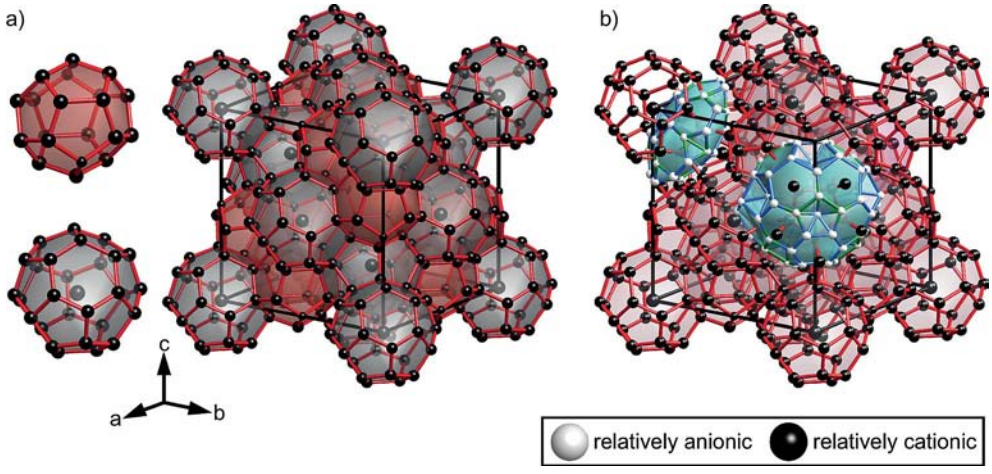

Figure 8. Extended D and TT networks in $Mg_{11}Cu_6Al_{12}$. (a) The relatively cationic D network of $Mg_{11}Cu_6Al_{12}$ forms a clathrate II framework, built from dodecahedra (red faces) and hexakaidecahedra (gray faces). (b) The relatively anionic TT network completes Friauf polyhedra around the D atoms. For clarity only a single Bergman cluster and hexagonal wheel of Friauf polyhedra are shown. See the caption to Figure 4 for plotting conventions.

can also be explained from this point of view as follows: in the process of building the TT network around the D atom dodecahedron and hexakaidecahedra, each TT presents triangular faces toward centers of the clathrate cages that it straddles. In the case of the dodecahedron, the TT triangles meet at the center to produce the central icosahedron of the Bergman cluster. In the case of the hexakaidecahedra, however, the TT triangles meet to create a Friauf polyhedron. This can explained in a different way: the Bergman cluster can be created by beginning with a central icosahedron and fusing each of its faces with the triangular face of the TT of Friauf polyhedra (allowing, of course, for the Friauf polyhedra to interpenetrate). The cluster of Friauf polyhedra surrounding the hexakaidecahedron can be constructed in a similar way, only this time the nucleus of the cluster is a Friauf polyhedron. The Mg2 site lies at the core of this central Friauf polyhedron.

We thus arrive at a simple quantum mechanically-derived view of the structural transition between the crystal structures of $Mg_{17}Al_{12}$ and $Mg_{11}Cu_6Al_{12}$. Upon the rotation of half of the $MgCu_2$-type clusters in $Mg_{17}Al_{12}$ as shown in Figure 2, the ambiguous atoms at the cluster interfaces snap into clear D and TT identities. The result is a structure that consists of D and TT networks extending throughout the crystal, as in Laves structures such as the $MgCu_2$ and $MgZn_2$ types. The difference lies in the way these networks are arranged. Whereas the D networks of the $MgCu_2$ and $MgZn_2$ types trace out the simple cubic diamond and hexagonal diamond structures, the D network of $Mg_{11}Cu_6Al_{12}$ traces out a more complex array of tetrahedra: the same clathrate network noted by Lin and Corbett in the nearly analogous structure of $Mg_{35}Cu_{24}Ga_{53}$.[25] The TT networks grow around this clathrate scaffold, providing each D site with a truncated tetrahedron. This process forms the polyhedra at the centers of the clathrate cavities: an icosahedron and a Friauf polyhedron of TT atoms at the cores of the dodecahedral and hexakaidecahedral cavities, respectively. The latter has space for hosting one additional D atom.

In the course of the $Mg_{17}Al_{12}$ to $Mg_{11}Cu_6Al_{12}$ transformation, six ambiguous positions/formula unit develop TT character with relatively anionic relative Mulliken populations. This is the just the number of sites needed to host the six Cu atoms that substitute for Mg on going from $Mg_{17}Al_{12}$ to $Mg_{11}Cu_6Al_{12}$. When we recall that the GGA-DFT results presented in the last section suggest that both structure types meet the stability criterion of a pseudogap close to the E_F for the $Mg_{11}Cu_6Al_{12}$ composition, the emergence of new sites with affinity for the relatively electronegative Cu atoms in the $Mg_{11}Cu_6Al_{12}$ composition presents itself as an important driving force for the structural transformation.

X. Conclusions

In this paper, we have taken a long structural journey in tracing the connections between two phases with great structural and compositional similarities, $Mg_{17}Al_{12}$ and the newly determined phase $Mg_{11}Cu_6Al_{12}$. The structures were of such similarity, differing only in the relative orientation of their clusters and the site occupancies of some sites, that we felt compelled to explore why $Mg_{11}Cu_6Al_{12}$ adopted its structure rather than the considerably simpler one of $Mg_{17}Al_{12}$. GGA-DFT calculations revealed that for the stoichiometry in question both structures offer a pseudogap at the Fermi energy. This is suggestive of an electronic origin to the stability of $Mg_{11}Cu_6Al_{12}$, but offers little in terms of explaining what features of its crystal structure make it preferable to that of $Mg_{17}Al_{12}$.

A clearer picture was found in relative Mulliken population analyses of elemental models of these structures. In examining the patterns of relatively anionic and cationic sites resulting from these calculations, a startling picture surfaced. The simplest of geometrical permutations – a 90° rotation of half of the $Mg_{17}Al_{12}$ structure's $MgCu_2$-type clusters – leads to profound electronic consequences: constructive interference between network types at the cluster interfaces leads to a new patterning of cationic and anionic sites. Now rather than $MgCu_2$-type clusters, with polar cores isolated from each other by non-polar interfaces, a continuous D network of cationic sites extends through the whole crystal. This is the very clathrate II network of cations identified by Lin and Corbett in their structural analysis of the nearly isostructural $Mg_{35}Cu_{24}Ga_{53}$.[25] The anionic sites also now make an extended network, built from face-sharing truncated tetrahedra, each of which surrounds a D site. Together, the TT and D neworks create an extended array of Friauf polyhedra that includes Bergman clusters and hexagonal wheels.

In the process of this electronic metamorphosis between the structures of $Mg_{17}Al_{12}$ and $Mg_{11}Cu_6Al_{12}$, the Mg sites with blurred identities in the former take on clear roles in the latter. Half of these sites become strongly cationic, with a clear affinity for relatively electropositive atoms. The other half now register as clearly anionic, to be preferred by more electronegative atoms. The nascent anionic sites accommodate the relatively electronegative Cu atoms as the Mg atoms of $Mg_{17}Al_{12}$ are replaced with Cu to attain the $Mg_{17-x}Cu_xAl_{12}$ ($x = 6$) composition of $Mg_{11}Cu_6Al_{12}$.

In this way, Mulliken population analysis reveals one driving force that may be at work in the formation of this $2 \times 2 \times 2$ superstructure of $Mg_{17}Al_{12}$. These results contribute to an emerging theme in the structural chemistry of complex intermetallics: while the complete bonding picture for individual phases may be complicated and subtle, the formation of superstructures from them often has simple, traceable origins.[32] We hypothesize that a similar mechanism of breaking site ambiguities to accommodate changes in the balance of relatively electropositive and electronegative atoms may play a role in the structural preferences of other intermetallic systems. Indeed, elemental substitution in intermetallic structures exhibiting ambiguous sites (as revealed in a Mulliken population analysis) may be one approach to the synthesis of new complex structures.

Experimental Section

Syntheses: The synthesis of $Mg_{11}Cu_6Al_{12}$ evolved from our pursuit of the $Mg_6Cu_3Al_7$ phase reported in the phase diagrams of the Al-Mg-Cu system.[15–17] The phase diagrams suggested that the preparation of $Mg_6Cu_3Al_7$ would be challenging, as this composition lies beneath the primary phase field for either a $MgCu_2$-type phase, or more a complex Laves phase, depending on the phase diagram. Stoichiometric preparations are then expected to create substantial amounts of Laves phases in addition to the phase of interest. Two synthetic approaches were then taken, one aiming for optimal crystallinity, the other for phase purity. Both approaches involving direct reaction of elements (aluminum, Alfa Aesar, 99.97% metals basis, powder –100+325 mesh; copper, Alfa Aesar, 99.5% metals basis, powder –150 mesh; magnesium, Sigma–Aldrich, 99.98% trace metals basis, chips 4–30 mesh; all used as received). The elements were weighed out in an Ar-filled glovebox into 0.876 cm diameter tantalum vessels, which were then welded shut with an arc-melting furnace and sealed into evacuated fused silica ampoules.

The two synthetic approaches differed in their nominal compositions and temperature profiles. Approach 1 aimed for crystals for single crystal studies, and involved slow cooling from a melt in the primary phase field of $Mg_6Cu_3Al_7$. The samples were placed in a muffle furnace, and the temperature was raised to 550°C and held there for 24 h. The furnace was then cooled to a rate of 1 °C per hour to 450°C, where the samples were annealed for 165 h. Approach 2 aimed for phase pure samples to confirm stoichiometry. In this approach near-stoichiometric mixtures were heated in a muffle furnace to 1000 °C to melt all components and held there for 5 h. The sealed quartz ampoules were then transferred directly to an ice water bath. The samples were resealed in new evacuated fused silica ampoules, and returned to the furnace at 500 °C to anneal for 357 h.

Both approaches resulted in shiny grey ingots. These were brittle, crushing easily in an agate mortar and pestle to yield shards for single crystal analysis. Further grinding resulted in fine powders for analysis with powder X-ray diffraction. No oxidation was evident after weeks in air, suggesting that the samples contain no substantial quantities of air sensitive phases.

Powder X-ray Diffraction: Powder X-ray diffraction data for phase purity assessment and unit cell parameter refinement were collected on a Scintag Pad V diffractometer with Cu-K_α radiation (λ = 1.54051 Å). Diffraction intensities were collected as a function of the diffraction angle (2θ) in steps of 0.02 degrees, with dwell times of 4.0 sec. Peaks were fit with Pearson VII profiles using the program *XFIT*,[33] and unit cell parameters were refined with the program *UNITCELL*.[34]

Elemental Analysis Using Energy Dispersive X-ray Spectroscopy (EDS): For determination of the elemental compositions of the phases synthesized, portions of the crushed samples were suspended in non-conductive epoxy, hand-polished against silicon carbide and diamond papers to create a flat surface, and coated with 250 nm of graphitic carbon. The polished samples were then inspected with a Hitachi S-3100N scanning electron microscope fitted with an EDS probe (voltage: 15 kV). Measurements at several points revealed the presence of only the three elements expected. Two phases were observed, but further analysis was necessary for certainty in elemental quantification.

Elemental Analysis Using Wavelength Dispersive X-ray Spectroscopy (WDS): The same polished samples were used for both EDS and WDS. Prior to WDS analysis, the samples were repolished to further reduce the amount of surface scratching. To ensure conductivity, carbon paint (graphite in 2-propanol) was applied to the epoxy immediately surrounding exposed grains. The samples were then inspected with a Cameca SX-51 electron microprobe (voltage: 15 kV). Several choices of standards were tested. The Mg/Al ratio was consistent for all of these choices, but sums of the percentages were closest to 100% when the following standards were employed: $MgAl_2O_4$ for Mg, Cu metal for Cu, and a 50:50 Al-Ni alloy for Al. Measurements at several points again revealed the presence of two phases, with the compositions $Mg_{32(2)}Cu_{38(4)}Al_{30(6)}$ (average of 5 measurements), and $Mg_{11.30(11)}Cu_{6.00(9)}Al_{12.86(11)}$ (average of 7 measurements).

Single Crystal X-ray Diffraction Measurements: A plate-shaped crystal was selected for single-crystal studies with dimensions $0.14 \times 0.05 \times 0.02$ mm^3 (see Table 1 for further details on the crystal). X-ray diffraction intensities were collected on an Oxford Diffraction XCalibur E Diffractometer with a Mo-K_α sealed-tube X-ray source (λ = 0.71069 Å). ω-scans were used to collect nearly a quadrant of reciprocal space out to 0.6 Å resolution. Run list optimization, as well as all steps of the data processing to create a list of integrated peak intensities, including the peak search, unit cell determination and refinement, the creation of reciprocal reconstructions, absorption correction, and frame scaling were carried out with the program *CrysalisPro* v. 171.[35] Structure solution was performed using the charge-flipping algorithm[36,37] with the program *SUPERFLIP*,[38] and the subsequent refinement of the crystal structure was carried out with the program *JANA2006*.[39]

Table 1. Crystal data, and details of data collection and structure refinement.[40]

Chemical formula	$Mg_{11}Cu_6Al_{12}$
WDS composition	$Mg_{11.30(11)}Cu_{6.00(9)}Al_{12.86(11)}$
Space group/setting	$Fd\bar{3}m$ (No. 227)
a [Å]	20.1416(13)
Cell volume [Å^3]	8171.1(9)
Z	16
Calculated density [g/cm^3]	3.1608
Crystal dimensions [mm]	$0.14 \times 0.05 \times 0.02$
Crystal color	metallic grey
Data collection temperature	room temperature
Radiation source, λ [Å]	Mo-K_α, 0.7107
F(000)	7392
Absorption coefficient [mm^{-1}]	6.979
Absorption correction	analytical (method of Clark and Reid[41])
Min./max. transmission	0.427/0.887
θ_{min}, θ_{max}	3.35, 37.27
Number of reflections	15132
Unique reflections [all, $I > 3\sigma(I)$]	1044, 627
R_{int}[all, $I > 3\sigma(I)$]	4.25, 5.01
Number of parameters	34
$R[I > 3\sigma(I)]$, $R_w[I > 3\sigma(I)]$	2.26, 5.38
R(all), R_w(all)	5.17, 5.63
$S[I > 3\sigma(I)]$, S(all)	1.38, 1.11
$\Delta\rho_{max}$ (electrons/Å^3)	0.61
$\Delta\rho_{min}$ (electrons/Å^3)	–1.71

Initial Inspection of Single Crystal Data: Single crystal X-ray diffraction peak positions were fit well with a 20.1 Å metrically cubic unit cell (90.09% of reflections indexed). Analysis of both reciprocal lattice reconstructions of frame data, and R_{int} values for integrated intensities confirmed the cubic symmetry of the crystal, and offered good agreement with the Laue symmetry group $m\bar{3}m$. Inspection of systematic absences suggested F-centering, the presence of d-glides perpendicular to <100>, and n-glides perpendicular to <110>. All of these observations point to the space group $Fd\bar{3}m$

Table 2. Refined atomic coordinates and atomic displacement parameters for $Mg_{11}Cu_6Al_{12}$.

Site	Wyckoff Position	x	y	z	U_{eff}	Occupancy
Al1	96*g*	0.04592(3)	0.63883(4)	0.04592(3)	0.00896(16)	1.0
Al2	96*g*	0.04709(3)	0.85708(4)	0.04709(3)	0.00877(16)	1.0
Cu1	96*g*	0.164130(11)	0.664131(11)	0.002660(17)	0.01253(7)	1.0
Mg1	8*b*	0	0.5	0	0.0104(3)	1.0
Mg2	8*a*	0	0	0	0.0147(4)	1.0
Mg3	32*e*	0.09325(5)	0.40675(5)	0.09325(5)	0.01040(17)	1.0
Mg4	32*e*	0.08508(5)	0.08508(5)	0.08508(5)	0.01156(18)	1.0
Mg5	96*g*	0.19059(3)	0.80941(3)	0.00491(5)	0.01275(19)	1.0
Site	U_{11}	U_{22}	U_{33}	U_{12}	U_{13}	U_{23}
Al1	0.0093(2)	0.0082(4)	0.0093(2)	0.0021(2)	0.0012(3)	0.0021(2)
Al2	0.0094(2)	0.0074(4)	0.0094(2)	–0.00020(19)	–0.0018(3)	–0.00020(19)
Cu1	0.01389(11)	0.01389(11)	0.00980(16)	–0.00382(12)	0.00026(9)	0.00026(9)
Mg1	0.0104(6)	0.0104(6)	0.0104(6)	0	0	0
Mg2	0.0147(6)	0.0147(6)	0.0147(6)	0	0	0
Mg3	0.0104(3)	0.0104(3)	0.0104(3)	–0.0007(4)	0.0007(4)	–0.0007(4)
Mg4	0.0116(3)	0.0116(3)	0.0116(3)	–0.0010(3)	–0.0010(3)	–0.0010(3)
Mg5	0.0130(3)	0.0130(3)	0.0122(4)	0.0009(3)	0.0001(3)	–0.0001(3)

(no. 227). This choice was confirmed by the results of the structure solution and refinement.

Structure Solution and Refinement: Application of the charge-flipping algorithm to integrated intensities quickly converged to a sharp electron density map consistent with $Fd\bar{3}m$ symmetry. Peak positions corresponded to the $K_{17}In_{41}$ structure type (Figure 1). From the electron densities at the peaks, a moderately clear separation of the three elements Cu, Al and Mg was evident: one large peak with density ϱ = 148.96 electrons/Å^3 was assigned to Cu, two smaller peaks with densities in the range ϱ = 68.95–66.86 were tentatively assigned to Al, and five peaks distributed in the range in ϱ from 60.62 to 48.17 were then attributed to Mg. An isotropic refinement was then carried out on F^2 leading to $R[I > 3\sigma(I)] = 5.00$ and reasonably consistent atomic displacement parameters (ADPs). Upon moving to an anisotropic refinement and adding an extinction correction, the $R[I > 3\sigma(I)]$ decreased to 2.26. No outstanding peaks were seen in the Fourier difference map. The resulting atomic coordinates and ADPs are listed in Table 2.

Having obtained the atomic positions, we then turned to finalization of the assignment of elements to sites. The electron counts of Al and Mg differ by only one (about 8%), so these are expected to be difficult to distinguish using X-ray diffraction data. Analysis of the interatomic distances (Table 3) was used to assess the plausibility of our initial assignments. Common Al–Al, Mg–Mg, Al–Mg, Al–Cu, and Mg–Cu contact lengths were analyzed with histograms generated by the Inorganic Crystal Structure Database (ICSD).[42–44] The common ranges for these contacts are found to be 2.6–3.1 Å for Al–Al, 2.9–3.3 Å for Mg–Mg, 3.0–3.3 for Al–Mg, 2.4–2.8 Å for Al–Cu, and 2.6–3.0 Å for Mg–Cu. All of the distances in Table 3 fall within these expected ranges, with the exception of those involving Mg4. This site exhibits coordination by six Al2 sites at distances of 3.00 Å, one Mg2 site at 2.97 Å and one Mg4 site at 2.785. The Mg4–Al2 distances could be consistent with either rather short Mg–Al contacts or long Al–Al contacts. The Mg2–Mg4 distance, likewise could be interpreted as either a short Mg–Mg or an average Mg–Al contact. The Mg4–Mg4 contact distance is similarly ambiguous: 2.785 Å lies in the near the peak of Al–Al distances in the ICSD histograms, but is very short for a Mg–Mg contact. However, such short Mg–Mg distances have been

Table 3. Selected interatomic distances for $Mg_{11}Cu_6Al_{12}$.

Site	Neighbor	Distance [Å]
Al1	Al1	2.6160(8)
	Al1(×2)	2.6464(10)
	Cu1(×2)	2.5861(7)
	Cu1	2.4641(8)
	Mg1	3.0870(8)
	Mg3(×2)	3.0998(12)
	Mg5(×2)	3.0258(11)
Al2	Al2	2.6827(8)
	Al2(×2)	2.7297(10)
	Cu1	2.4710(9)
	Mg2	3.1758(8)
	Mg3	3.1360(11)
	Mg4(×2)	3.0049(11)
	Mg5(×2)	3.1619(10)
	Mg5(×2)	3.1226(11)
Cu1	Al2	2.4710(9)
	Al1(×2)	2.5861(7)
	Al1	2.4641(8)
	Mg3	2.7943(10)
	Mg5(×2)	2.9746(8)
	Mg5(×2)	2.9447(9)
Mg1	Al1(×12)	3.0870(8)
	Mg3(×4)	3.2532(10)
Mg2	Al2 (×12)	3.1758(8)
	Mg4(×4)	2.9682(10)
Mg3	Al1(×6)	3.0998(12)
	Al2(×3)	3.1359(11)
	Cu1(×3)	2.7943(10)
	Mg1	3.2532(10)
	Mg5(×3)	3.2066(14)
Mg4	Al2(×6)	3.0049(11)
	Mg2	2.9682(10)
	Mg4	2.7852(13)
Mg5	Al1(×2)	3.0258(11)
	Al2(×2)	3.1619(10)
	Al2(×2)	3.1226(11)
	Cu1(×2)	2.9746(8)
	Cu1(×2)	2.9446(9)
	Mg3	3.2066(14)
	Mg5(×2)	3.2152(11)

observed previously in intermetallics,[45–48] such as 2.7664 Å in Mg_2Cu,[48] and 2.6083 Å in MgIr.[47]

For resolution of the assignment of Mg4, we turned to other experimental information. The assignment of Mg4 as Mg or Al leads to different overall compositions: $Mg_{11}Cu_6Al_{12}$ and $Mg_9Cu_6Al_{14}$, respectively. These numbers can be compared to the composition from WDS as $Mg_{11.30(11)}Cu_{6.00(9)}Al_{12.86(11)}$, whose Mg/Al ratio favors the former stoichiometry. Further evidence can be found from the single crystal data; refinement of the structure with Mg4 occupied by Al leads to a U_{eff} value nearly 2.5 times that of the other Al sites with little change in the R-factor relative to the original model. The large U_{eff} suggests that model's electron density on that site is too high when Al is placed on that site, consistent with the site being occupied by Mg. Final confirmation of the assignment of Mg4 as Mg comes from the powder X-ray diffraction patterns of samples with nominal compositions of $Mg_{11}Cu_6Al_{12}$ and $Mg_9Cu_6Al_{14}$, both of which were first heated to 1000° for 5 h, followed by quenching in cold water, and then annealing at 500 °C for 357 h. While both showed the presence of impurity phases, particularly $MgZn_2$-type Laves phases (see above), the qualitative yield of the target phase was higher for the $Mg_{11}Cu_6Al_{12}$ composition. For these reasons, the Mg4 site was concluded to indeed be occupied by Mg. From the data available, however, we cannot rule out the possibility of some mixed occupancy with Al on this site.

Electronic Structure Calculations: All structure optimizations and the calculation of DOS curves were performed with the Vienna ab initio Simulation Package, at the GGA-DFT level with Projector Augmented Wave (PAW) potentials provided with the package.[49–54] The electronic structure calculations for $Mg_{11}Cu_6Al_{12}$ ($K_{17}In_{41}$ type), $Mg_{17}Al_{12}$ (α-Mn type) with half of the outermost D sites exchanged for Cu to attain the stoichiometry of $Mg_{11}Cu_6Al_{12}$, and $Mg_{17}Al_{12}$ were carried out in the high precision mode with energy cut-offs of 341.6, 341.6, and 300.5 eV, respectively. Optimizations of the unit cell volume, cell shape, and ion positions were performed in sequence using first a $5\times5\times5$ k point-mesh and then with a $9\times9\times9$ mesh. All degrees of freedom were then optimized simultaneously using the same series of point meshes. DOS curves were generated for the optimized structures using a $11\times11\times11$ k point-mesh for $Mg_{11}Cu_6Al_{12}$ in the $K_{17}In_{41}$ type and a $13\times13\times13$ k point-mesh for both α-Mn-type structures.

All Mulliken populations were extracted from extended Hückel (eH) tightbinding calculations performed with the program YAeHMOP.[55] Mulliken populations were calculated for elemental models of both $Mg_{17}Al_{12}$ and $Mg_{11}Cu_6Al_{12}$ in which Al is placed on all sites. The Al atoms were modeled with an *sp* single zeta basis set of Slater Type Orbitals, and used parameters developed previously in the study of $Mg_{17}Al_{12}$: $H_{ii}(3s) = -12.5$ eV, $H_{ii}(3p) = -6.5$ eV, $\zeta(3s) = 1.267$ and $\zeta(3p) = 1.267$. These parameters were shown to reproduce the qualitative features of the LDA-DFT band structure of $Mg_{17}Al_{12}$.[10]

Acknowledgments

We thank Drs. John Fournelle and Hiromi Konishi at UW-Madison Dept. of Geosciences for their assistance with the EDS/WDS and powder X-ray diffraction measurements, respectively. We also gratefully acknowledge the financial support of the US DOE Office of Science Early Career Program (DE-SC0003947) through the Office of Basic Energy Sciences, and the University of Wisconsin through start-up funds.

[1] L. Pauling, *J. Am. Chem. Soc.* **1923**, *45*, 2777–2780.
[2] S. Samson, *Nature* **1962**, *195*, 259–263.
[3] S. Samson, *Acta Crystallogr.* **1964**, *17*, 491–495.
[4] S. Samson, *Acta Crystallogr.* **1965**, *19*, 401–413.
[5] S. Samson, *Acta Crystallogr.* **1967**, *23*, 586–600.
[6] T. Weber, J. Dshemuchadse, M. Kobas, M. Conrad, B. Harbrecht, W. Steurer, *Acta Crystallogr., Sect. B* **2009**, *65*, 308–317.
[7] M. Conrad, B. Harbrecht, T. Weber, D. Y. Jung, W. Steurer, *Acta Crystallogr., Sect. B* **2009**, *65*, 318–325.
[8] S. Andersson, *Acta Crystallogr., Sect. B* **1980**, *36*, 2513–2516.
[9] Q.-B. Yang, S. Andersson, L. Stenberg, *Acta Crystallogr., Sect. B* **1987**, *43*, 14–16.
[10] D. C. Fredrickson, S. Lee, R. Hoffmann, *Angew. Chem.* **2007**, *119*, 2004–2023; *Angew. Chem. Int. Ed.* **2007**, *46*, 1958–1976.
[11] P. Schobinger-Papamantellos, P. Fischer, *Naturwissenschaften* **1970**, *57*, 128–129.
[12] J.-C. Crivello, T. Nobuki, T. Kuji, *Intermetallics* **2007**, *15*, 1432–1437.
[13] S. Samson, E. K. Gordon, *Acta Crystallogr., Sect. B* **1968**, *24*, 1004–1013.
[14] M. Feuerbacher, J. P. A. Makongo, S. Hoffmann, R. Cardoso, Yu. Grin, G. Kreiner, J.-M. Joubert, S. Brühne, T. Proffen, W. Assmus, A. Czyrska-Filemonowicz, A. Zielinska-Lipiec, B. Dubiel, T. Schenk, J. Gastaldi, H. Nguyen-Thi, N. Mangelinck-Noël, B. Billia, P. Donnadieu, J. Christensen, S. Lidin, D. Fredrickson, M. Mihalkovic, T. Weber, P. Schaub, M. de Boissieu, F. Bley, W. Sikora, J. Malinowski, J. Schreuer, W. Steurer, *Z. Kristallogr.* **2007**, *222*, 259–288.
[15] A. Prince, G. Effenberg, *Ternary Alloys*, vol. 4, VCH, Weinheim, Germany, **1991**.
[16] T. Buhler, S. G. Fries, P. J. Spencer, H. L. Lukas, *J. Phase Equilib.* **1998**, *19*, 317–333.
[17] V. Raghavan, *J. Phase Equilib.* **2007**, *28*, 174–179.
[18] G. Cordier, V. Müller, *Z. Kristallogr.* **1993**, *205*, 353–354.
[19] G. Cordier, V. Müller, *Z. Naturforsch. B: Chem. Sci.* **1994**, *49*, 721–728.
[20] B. Li, J. D. Corbett, *Inorg. Chem.* **2003**, *42*, 8768–8772.
[21] M. S. Mirgalovskaya, *Dokl. Akad. Nauk SSSR* **1951**, *77*, 289–292.
[22] Z.-Q. Li, S.-Y. Zhang, B.-Y. Wu, *Mater. Sci. Technol.* **2001**, *17*, 465–471.
[23] X.-Z. Liu, M. Yang, Z.-H. Xing, X.-F. Ren, *Trans. Nonferrous Met. Soc. China* **2003**, *13*, 153–157.
[24] M. Tillard-Charbonnel, C. Belin, *Mater. Res. Bull.* **1992**, *27*, 1277–1286.
[25] Q. Lin, J. D. Corbett, *Inorg. Chem.* **2005**, *44*, 512–518.
[26] B. M. Gimarc, *J. Am. Chem. Soc.* **1983**, *105*, 1979–1984.
[27] H. C. Longuet-Higgins, C. W. Rector, J. R. Platt, *J. Chem. Phys.* **1950**, *18*, 1174–1181.
[28] G. J. Miller, *Eur. J. Inorg. Chem.* **1998**, 523–536.
[29] C. S. Lee, G. J. Miller, *Inorg. Chem.* **2001**, *40*, 338–345.
[30] J. T. Schmidt, S. Lee, D. C. Fredrickson, M. Conrad, J. Sun, B. Harbrecht, *Chem. Eur. J.* **2007**, *13*, 1394–1410.
[31] R. F. Berger, S. Lee, R. Hoffmann, *Chem. Eur. J.* **2007**, *13*, 7852–7863.
[32] D. C. Fredrickson, S. Lidin, G. Venturini, B. Malaman, J. Christensen, *J. Am. Chem. Soc.* **2008**, *130*, 8195–8214.
[33] A. A. Coelho, R. W. Cheary, *X-ray Line Profile Fitting Program, XFIT*, University of Technology, Sydney, Australia, **2007**.
[34] T. J. B. Holland, S. A. T. Redfern, *Mineral. Magazine* **1997**, *61*, 65–77.
[35] Oxford Diffraction, Oxford Diffraction Ltd., *Xcalibur CCD system*, v. 1.171.32, CrysAlisPro Software system, **2007**.
[36] G. Oszlanyi, A. Suto, *Acta Crystallogr., Sect. A* **2004**, *60*, 134–141.
[37] G. Oszlanyi, A. Suto, *Acta Crystallogr., Sect. A* **2005**, *61*, 147–152.

[38] L. Palatinus, G. Chapuis, *J. Appl. Crystallogr.* **2007**, *40*, 786–790.
[39] V. Petříček, M. Dušek, L. Palatinus, *Jana2006. The crystallographic computing system*, Institute of Physics, Praha, Czech Republic.
[40] A crystallographic information file containing further details of the crystal structure investigation of $Mg_{11}Cu_6Al_{12}$ may be obtained from the Fachinformationszentrum Karlsruhe, 76344 Eggenstein-Leopoldshafen, Germany (Fax: +49-7247-808-666; E-mail: crysdata@fiz-karlsruhe.de), on quoting the depository number CSD-422849.
[41] R. C. Clark, J. S. Reid, *Acta Crystallogr., Sect. A* **1995**, *51*, 887–897.
[42] G. Bergerhoff, I. D. Brown, in: *Crystallographic Databases* (Ed.: F. H. Allen et al.), Chester, International Union of Crystallography, **1987**.
[43] A. Belsky, M. Hellenbrandt, V. L. Karen, P. Luksch, *Acta Crystallogr., Sect. B* **2002**, *58*, 364–369.
[44] J. A. Kaduk, *Phys. Rev. B* **2002**, *58*, 370–379.
[45] R. Ferro, G. Rambaldi, *J. Less-Common Met.* **1960**, *2*, 383–391.
[46] R. Ferro, G. Rambaldi, R. Capellt, *J. Less-Common Met.* **1962**, *4*, 16–23.
[47] R. Černý, G. Renaudin, V. Favre-Nicolin, V. Hlukhyy, R. Pöttgen, *Acta Crystallogr., Sect. B* **2004**, *60*, 272–281.
[48] M. H. Braga, J. J. A. Ferreira, J. Siewenie, T. Proffen, S. C. Vogel, L. L. Daemen, *J. Solid State Chem.* **2010**, *183*, 10–19.
[49] G. Kresse, J. Hafner, *Phys. Rev. B* **1993**, *47*, 558–561.
[50] G. Kresse, J. Hafner, *Phys. Rev. B* **1994**, *49*, 14251–14269.
[51] G. Kresse, J. Furthmüller, *Comput. Mater. Sci.* **1995**, *6*, 15–50.
[52] G. Kresse, J. Furthmüller, *Phys. Rev. B* **1996**, *54*, 11169–11186.
[53] P. E. Blöchl, *Phys. Rev. B* **1994**, *50*, 17953–17979.
[54] G. Kresse, D. Joubert, *Phys. Rev. B* **1999**, *59*, 1758–1775.
[55] G. A. Landrum, *YAeHMOP: Yet Another extended Hückel Molecular Orbital Package*, v. 3.0.; YAeHMOP is freely available on the WWW: http://sourceforge.net/projects/yaehmop/.

Received: March 29, 2011
Published Online: June 17, 2011

